XPS investigation of Mn valence in lanthanum manganite thin films under variation of oxygen content

Elke Beyreuther,* Stefan Grafström, and Lukas M. Eng

Institute of Applied Photophysics, Technische Universität Dresden, D-01062 Dresden, Germany

Christian Thiele and Kathrin Dörr

Institute for Metallic Materials, IFW Dresden, D-01171 Dresden, Germany

The question whether $LaMnO_3$ accepts doping with tetravalent cations such as cerium and thus allows the preparation of electron-doped mixed-valent lanthanum manganites has been discussed controversially so far. Against the background of this problem, we present a comparative x-ray photoemission (XPS) study of epitaxial $La_{0.7}Ce_{0.3}MnO_3$ (LCeMO) and $La_{0.7}Ca_{0.3}MnO_3$ (LCMO) thin films. We focus on the exchange splitting of the Mn $3s$ core level peak, which is a direct indicator of the Mn valence and allows us to quantify the Mn valence in the outermost 3 nm of the films. We demonstrate that, depending on the oxygen content, the Mn valence can be tuned between a mixed $Mn^{3+/4+}$ state and a mixed $Mn^{2+/3+}$ state in *both* the LCeMO *and* the LCMO film. The oxygen content was varied by heating in ultrahigh vacuum for deoxygenation and in an oxygen atmosphere for reoxidation. In the LCeMO film, the deoxygenation not only changes the Mn valence, but also the Ce valence is driven from the 4+ towards the 3+ state.

I. INTRODUCTION

Doped lanthanum manganites of the general formula $La_{1-x}A_xMnO_3$ (A=divalent or tetravalent cation) exhibit a wide variety of magnetic, electronic, and crystallographic phases because of the complex interplay between charge, spin, and orbital degrees of freedom.[1–3] The discovery of the colossal magnetoresistance (CMR) effect in those compounds[4] motivated many research efforts not only from the fundamental but also from the application-related point of view.

So far, the majority of the reported research activities have been dedicated to hole-doped manganites in which part of the trivalent La ions of the parent compound $LaMnO_3$ have been replaced by *divalent* cations such as Sr^{2+}, Ca^{2+}, Ba^{2+}, Pb^{2+}, etc. Formally, this results in the chemical composition $(La_{1-x}^{3+}A_x^{2+})(Mn_{1-x}^{3+}Mn_x^{4+})O_3$. To preserve charge neutrality, part of the Mn ions are driven into the 4+ state which leads to an effective hole doping, where the conduction mechanism is based on electron hopping between the Mn^{3+} and Mn^{4+} ions via an oxygen ion, known as double exchange.

In analogy, from the aspect of possible manganite-based electronic devices, it is logical to ask whether a partial substitution of the La ions by *tetravalent* cations such as Ce or, so far less studied, Sn,[5–7] Te,[8–11] Zr,[12] Th[13] would lead to an electron-doped compound. Straightforward, one then expects the nominal composition $(La_{1-x}^{3+}A_x^{4+})(Mn_{1-x}^{3+}Mn_x^{2+})O_3$, where part of the Mn ions have been driven to the Mn^{2+} state. However, as the Mn^{2+} ion has a large ionic radius and the tetravalent ions have, compared with La^{3+}, a small radius, the question was raised whether such a crystal can be chemically stable at all.[13] Nevertheless, the hope has been that the physics (including double exchange and strong electron-lattice coupling) of those new compounds would be similar to that of hole-doped manganites. Thus, also the tetravalent-ion-doped manganites are expected to show all the unusual physical properties, including the CMR effect. Band structure calculations[14] supported the argument that a mixed $Mn^{2+/3+}$ state could be possible.

Several groups[15–17] succeeded in synthesizing Ce-doped manganites via a solid-state reaction route and reported evidence for metal-insulator and ferromagnetic-paramagnetic phase transitions, as well as for a CMR effect. On the other hand, the new manganites often suffered from overoxygenation,[15] and their properties turned out to be much more sensitive to the oxygen content and thus to the preparation conditions[18,19] than those of their hole-doped relatives. Even worse, accurate x-ray diffraction (XRD) analyses showed that the compounds always included an unreacted CeO_2 (or SnO_2 etc.) impurity phase or were generally a multiphase compound of self-doped $La_{1-x}MnO_3$, CeO_2, and Mn_3O_4,[13] or an even more complex mixture.[20] Ganguly *et al.*[21] generally questioned the possibility of Ce doping of $LaMnO_3$ and argued that the observed CMR effect and the metallic conductivity originated from a La-deficient $La_{0.7}MnO_3$ phase, motivated by work of Philip *et al.*[22] who gave evidence of hole rather than electron doping from thermopower measurements. Other researchers suggested that mixtures of $Ce^{3+/4+}$ *and* $Mn^{2+/3+/4+}$ would be possible,[22,23] demonstrated the existence of Mn^{2+} ions in hole-doped $La_{0.7}Sr_{0.3}MnO_3$,[24] or generally questioned the well established $Mn^{3+/4+}$ picture.[25]

At least the problem of phase separation seemed to be solved when Raychaudhuri *et al.*[26] and Mitra *et al.*[27,28] succeeded in preparing single-phase epitaxial LCeMO *thin films* by pulsed-laser deposition (PLD) which opened the way to lanthanum-manganite-based *pn* junctions[29,30] or tunneling magnetoresistance (TMR) structures.[31]

In order to directly or indirectly prove the expected electron doping, numerous more or less elaborate experi-

mental approaches have been followed so far, among them Hall measurements,[6,32,33] co-doping with divalent ions combined with resistance measurements,[26] thermopower measurements,[10,22] x-ray absorption spectroscopy (XAS),[34–36] x-ray photoemission spectroscopy (XPS),[6,8,34,36] or x-ray absorption near-edge-structure (XANES) spectroscopy.[37,38]

Up to the present, all those studies have almost alternately brought indications for either hole or electron doping in tetravalent-ion-doped manganites, in bulk samples as well as in epitaxial thin films. It is an aggravating fact that an impurity-free XRD pattern does not necessarily mean that the compound shows *n*-type conduction.[33] Obviously, the question whether $LaMnO_3$ accepts electron doping has to be answered for each sample individually.

In this work, we propose the application of XRD to ensure single-phase composition (as a necessary but not sufficient constraint) followed by an extensive XPS analysis, which provides information *both* on the valence states of the Mn and tetravalent ions *and* on the chemical composition of the outermost 3 nm of the films. The latter gives information on the oxygen content and on possible surface segregation. We have comparatively studied LCeMO and LCMO epitaxial thin films and show how the analysis of the XPS peak areas and the exchange splitting of the Mn 3*s* core level signal, which is a definite indicator for the Mn valence[39–41] and has so far only sporadically been applied to the problem of electron- and hole-doped manganites,[9,42,43] makes possible a clear analysis of the oxygen content and a quantitative determination of the Mn valence. We show that the oxygen content can be varied by heating in ultrahigh vacuum or in an oxygen atmosphere and that this allows us to tune the Mn valence in a reversible way.

II. EXPERIMENTAL

Epitaxial films of 10 nm thick $La_{0.7}Ca_{0.3}MnO_3$ (LCMO) and $La_{0.7}Ce_{0.3}MnO_3$ (LCeMO) were deposited on $SrTiO_3(100)$ single-crystal substrates by pulsed-laser deposition in off-axis geometry.[29,44] The stoichiometric targets were ablated with a KrF excimer laser at a wavelength of 248 nm.

XRD measurements were employed to ensure single-phase epitaxial growth. All films were aditionally characterized by atomic force microscopy (AFM) in the contact mode (Park Scientific, AutoProbe M5). The AFM measurements revealed films with a root mean square (rms) roughness of 1 and 2 nm for LCeMO and LCMO, respectively, as extracted from scan areas of 4 μm^2 (see Fig. 1). Both films grew in an island-type way on the $SrTiO_3(100)$ substrates.

XPS measurements were performed with an x-ray source (Leybold RQ 63-10) equipped with an Mg anode (hν =1253.6 eV) and a hemispherical energy analyzer (Leybold EA 10) in an ultrahigh vacuum (UHV) chamber at a base pressure of 10^{-10} mbar. The work function of the analyzer was calibrated with the spectrum of a Au(110) single-crystal surface, which had been cleaned by repeated cycles of heating and Ar$^+$ sputtering.

Prior to each XPS session, special attention was paid to the surface cleaning of the samples. Several reports[43,45–47]
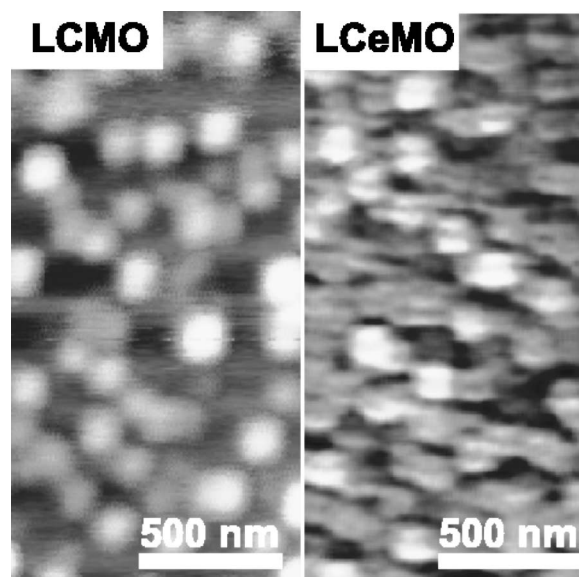
FIG. 1. Contact-AFM topographs of the LCMO and the LCeMO film. The black-to-white contrast corresponds to a height of 12 nm for LCMO and 6 nm for LCeMO.

suggest a heating procedure at 450 °C or 500 °C in UHV. To our experience, this does not completely remove carbon contaminants; the carbon 1*s* core level peak was still observable in the XP spectra after such a treatment. This fact is not astonishing since lanthanum manganite surfaces act as catalysts,[48–51] which demonstrates their high chemical reactivity. Therefore, we employed cycles of repeated heating at 470 °C for at least 2 h at an oxygen pressure of 10^{-6} mbar. Heating in an oxygen atmosphere is a common method for the UHV preparation of reactive surfaces such as platinum as it oxidizes the carbon on the surface to CO_2, which subsequently more easily desorbs from the surface. In the case of lanthanum manganites as well as other metal oxides, the oxygen plays another important role: It prevents oxygen diffusion[52] out of the samples. After each cleaning procedure, it was checked that the C 1*s* signal had disappeared. Typically, the freshly prepared surfaces remained clean for at least four hours.

The core level peaks with the highest intensities, i.e., La 3*d*, O 1*s*, Mn 2*p*, and Ca 2*p* or Ce 3*d* for LCMO or LCeMO, respectively, were acquired with an energy resolution of 2 eV, which corresponds to an analyzer pass energy of 70 eV, and with a step width of 0.2 eV and a measurement time of 10 s per step. The Mn 3*s* line, which is much weaker than the Mn 2*p* line, was scanned with a higher pass energy of the analyzer of 100 eV, which resulted in a slightly worse energy resolution of 2.5 eV. The measurement window was enlarged to 60 s per scan step to improve the signal-to-noise ratio. Unfortunately, the smaller peak of the Mn 3*s* doublet is located within the direct neighborhood of the Mg $K\alpha_{3,4}$ satellites of the La 4*d* signal (see Fig. 2). Consequently, the whole La 4*d* region of the spectrum had to be measured additionally in order to deconvolute the several contributions and to find the correct level for the correction of the inelastic background. For the evaluation of the XPS data, the Shirley background correction[53] and the peak fitting software XPS-
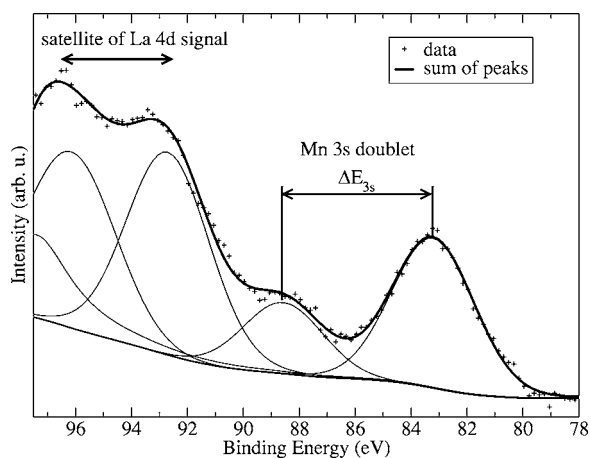
FIG. 2. Mn $3s$ core level signal and La $4d$ satellite signal for the LCeMO thin film on SrTiO$_3$(100) with corresponding peak fits and Shirley background. The La $4d$ satellite is fit by a four-peak structure (the fourth peak is outside the shown binding energy range) as suggested in Ref. 56.

PEAK 4.1[54] were used. The integral peak areas of the most intensive peaks were employed to calculate the concentration ratios between the elements of each compound within the XPS probing depth according to the relation:

$$\frac{c_A}{c_B} = \frac{I_A}{I_B}\frac{s_B}{s_A}. \tag{1}$$

Here, c_A and c_B are the concentrations of atoms of types A and B, I_A and I_B denote the XPS peak areas after background correction, and s_A and s_B are the empirically derived atomic sensitivity factors for an energy analyzer whose transmission function varies with the inverse of the electron kinetic energy, taken from Ref. 55.

On the basis of the measured Mn $3s$ level splitting ΔE_{3s}, the Mn valence v_{Mn} was calculated by employing the following linear equation:

$$v_{Mn} = 9.67 - 1.27\Delta E_{3s}/\text{eV}, \tag{2}$$

which was obtained by averaging the results of Refs. 39 and 40, where the linear relationship between v_{Mn} and ΔE_{3s} is derived for the valence range between +2 and +4 from XPS investigations of different bulk mixed-valent manganites and of binary Mn oxides, respectively. For comparison, we also calculate the Mn valence from the film stoichiometries as extracted from the peak area analysis.

The XP spectra were acquired after seven different sample treatment steps (see Table I) in order to compare the Mn valences for various stoichiometries, especially several degrees of oxygen deficiency. Step a denotes the pure cleaning procedure. Steps $b−f$ contain a cleaning procedure in an oxygen atmosphere followed by a deoxygenation procedure without oxygen supply at different heating temperatures and variable durations. Step g was applied in order to reoxidize the manganite films to restore the state that had been reached after step a. The temperatures are approximate values since the sample temperature was measured by an optical pyrometer (Impac, IGA 100) without exact knowledge of the emis-

TABLE I. Description of the seven different surface treatment steps applied to the LCMO and LCeMO thin films. Note that the original as-cleaned state of the films was reestablished by heating in an oxygen atmosphere *before* each new deoxygenation step (cf. Sec. III F).

Index	Sample treatment
a	470 °C, 2 h, 10^{-6} mbar O$_2$
b	470 °C, 2 h, 10^{-6} mbar O$_2$/470 °C, 1 h, UHV
c	470 °C, 1 h, 10^{-6} mbar O$_2$/520 °C, 2 h, UHV
d	470 °C, 1 h, 10^{-6} mbar O$_2$/570 °C, 2 h, UHV
e	470 °C, 1 h, 10^{-6} mbar O$_2$/620 °C, 2 h, UHV
f	470 °C, 1 h, 10^{-6} mbar O$_2$/670 °C, 2 h, UHV
g	470 °C, 3 h, 10^{-6} mbar O$_2$ (reoxidation)

sivity of the manganite films. The emissivity was set to 0.8, which is a typical value for metal oxides.[57] The base pressure in the preparation chamber was 10^{-9} mbar.

Two additional test procedures were performed after steps a and f for both samples. First, the O $1s$ peak was acquired at four values of the intensity of the x-ray source differing by a factor of up to 3.5, to make sure that no spectral shift occurs when the total photoelectron current is changed. This proves that the films provide enough conductivity to prevent any charging that could cause artificial line shifts. Second, an ultraviolet photoelectron spectrum (UPS) was taken to monitor the change of the work function of the films.

III. RESULTS AND DISCUSSION

A. XPS peak areas and stoichiometry

The atomic ratios between the elements were estimated from the integral peak areas of the La $3d$, Ce $3d$, Ca $2p$, O $1s$, and Mn $2p$ core level signals on the basis of Eq. (1). The nominal compositions of the LCMO and the LCeMO films resulting from this procedure are listed in Table II. The nor-

TABLE II. Chemical compositions of the LCMO and LCeMO films after seven different treatment steps. For comparison, the nominal stoichiometry (as expected from the PLD targets) has been added in the last line. Note that the values refer only to the outermost few nanometers of the film and that the errors are estimated to be greater than 10%. Note also that for the film as a whole, a change of the concentrations of the metal ions is not expected.

Index	LCMO	LCeMO
a	La$_{0.32}$Ca$_{0.20}$MnO$_{2.31}$	La$_{0.41}$Ce$_{0.21}$MnO$_{2.73}$
b	La$_{0.31}$Ca$_{0.22}$MnO$_{2.30}$	La$_{0.39}$Ce$_{0.19}$MnO$_{2.32}$
c	La$_{0.33}$Ca$_{0.21}$MnO$_{1.88}$	La$_{0.39}$Ce$_{0.20}$MnO$_{2.35}$
d	La$_{0.34}$Ca$_{0.22}$MnO$_{2.14}$	La$_{0.50}$Ce$_{0.19}$MnO$_{2.43}$
e	La$_{0.35}$Ca$_{0.20}$MnO$_{1.77}$	La$_{0.43}$Ce$_{0.14}$MnO$_{1.80}$
f	La$_{0.45}$Ca$_{0.25}$MnO$_{2.01}$	La$_{0.75}$Ce$_{0.27}$MnO$_{3.00}$
g	La$_{0.48}$Ca$_{0.32}$MnO$_{3.03}$	La$_{0.54}$Ce$_{0.21}$MnO$_{2.96}$
	La$_{0.70}$Ca$_{0.30}$MnO$_{3.00}$	La$_{0.70}$Ce$_{0.30}$MnO$_{3.00}$

malization to manganese is arbitrary. Note that the compositions of Table II are valid provided that the depth probed by XPS is smaller than the film thickness, which is well fulfilled in our case, and under the assumption of homogeneous films. Furthermore, the values are subject to an estimated error of at least 10%, which is mainly caused by the uncertainty of the Mn $2p$ peak area and the error of the inelastic background correction.[58] The Mn $2p$ doublet is surrounded by several broad Ce, Mn, and La Auger lines (Ce $M_5N_{45}N_{45}$ at 594 eV, Mn $L_3M_{45}M_{45}$ at 620 eV, La $M_5N_{45}N_{45}$ at 632 eV, Mn $L_3M_{23}M_{45}$ at 670 eV).[59] Consequently, it is difficult to exactly isolate the pure Mn $2p$ peak area. That is the reason why the apparent Mn excess should not be overvalued. Further systematic errors occur due to the uncertainty of the atomic sensitivity factors of La, Ce, and Mn. This manifests a fundamental problem, as the atomic sensitivity factors for rare-earth and transition metal elements vary strongly for different valence and binding conditions.[55] We come back to this point later when discussing the formal Mn valences.

Nevertheless, for both film surfaces investigated here, there is a clear indication of oxygen loss from step a towards step e. The development between steps b and d is dominated by stoichiometry fluctuations without any clear tendency. After step g a considerable oxygen reuptake is observed. Here, the stoichiometries of both film surfaces agree even better with the stoichiometries of the PLD targets than after step a. Considering the La:O ratio, there is an oxygen excess after steps $a-d$ and again after step g for LCeMO and after all treatment steps for LCMO. Examining the La:Ce ratio in LCeMO, we observe a Ce excess after the treatment steps $a-f$, whereas the correct ratio is found after step g, to within the error margin. As for the La:Ca ratio in LCMO, we find an excess of Ca after steps $e-g$. This points to Ca segregation to the surface,[45,46,60] which is supported by the analysis of the O:Ca ratio, which also shows Ca excess (except for step g). It must be taken into account that the results of Table II are only valid within the XPS probing depth. A typical value for the inelastic mean free path of electrons in inorganic compounds at a kinetic energy of 1000 eV is 2 nm,[61] which means that 78% of the signal comes from the outermost 3 nm of the film.

In the following, we focus on the different core level signals in detail, which will also clarify the reasons for the strongly changed stoichiometry of the LCeMO film after step f.

B. The O $1s$ core level signal

Figure 3 presents the development of the O $1s$ signal for both investigated films after the first six steps of treatment as listed in Table I. Several tendencies can be observed: With increasing heating temperature and thus progressive oxygen loss, the O $1s$ signal moves towards higher binding energies and the peak height decreases slightly.

The correct interpretation of the manganite O $1s$ peak seems to be difficult as the literature contains many contradictory statements. Some groups[48,62] (however, those statements are for La$_{1-x}$Sr$_x$MnO$_3$) suggest three contributions to the O $1s$ signal and attribute them to the binding to each of
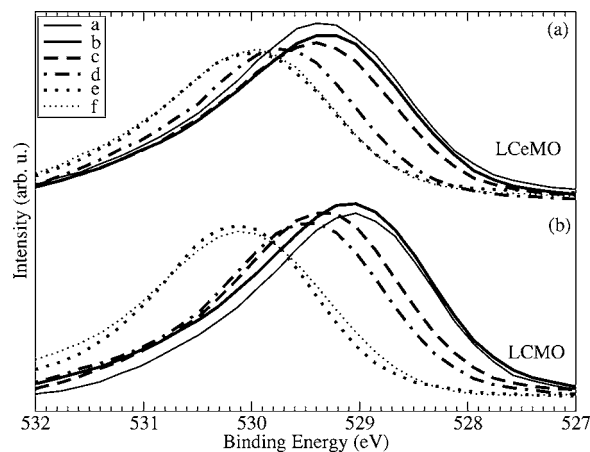
FIG. 3. O $1s$ core level signals after background subtraction for LCeMO (a) and LCMO (b). The legend refers to the treatment procedures of Table I. For the reason of visual clarity, the peaks corresponding to the reoxidized state (step g), which are almost congruent with the respective peaks after step a, are not shown in the diagram.

the three other elements of the compound. According to this interpretation, the Mn-O component is located at about 529 eV and the La-O component at about 531 eV. This would be consistent with the O $1s$ signals of the present work, but a third component at a higher binding energy, which could be attributed to Ca-O or Ce-O (analogously to Sr-O) cannot be found in our data. The peak can be well fit by two but not three lines.

Other groups[45,46,49,50] observe a two-peak structure, with a component attributed to lattice oxygen at lower binding energies and a component attributed to surface-or defect-related oxygen at higher binding energies. This interpretation is more consistent with the observations of the present work. Then, an increase of the lattice-to-surface oxygen ratio with increasing heating temperature can be stated. Unaffected by those controversial details, the O $1s$ peak is a more direct and thus more reliable indicator for the control of oxygen loss than the element ratios obtained from the peak area analysis.

C. Ce $3d$ and Ca $2p$ core level signals

The interpretation of Ce $3d$ spectra of Ce compounds has been the subject of a number of experimental and theoretical studies.[63–70] In general, the Ce $3d$ spectrum exhibits a spin-orbit splitting of 18.6 eV, which could be verified for the LCeMO film in the present work. Furthermore, both spin-orbit components show a multiplet splitting into either two components for the pure Ce^{3+} state, as in Ce$_2$O$_3$, (denoted as v_0, v', u_0, u') or three components (v, v'', v''', u, u'', u''') for the pure Ce^{4+} state, as in CeO$_2$. Consequently, for an arbitrary mixed-valence state, each of the two spin-orbit components must be fit by five peaks (see, for example, Ref. 71 and references therein). The percentages of Ce^{3+} and Ce^{4+} can then be determined by evaluating the peak areas attributed to the two different oxidation states. Figure 4 depicts the Ce $3d$ signals for the cleaned LCeMO surface (step a) and after heating at 620 °C (step e). The cleaned film shows, as ex-
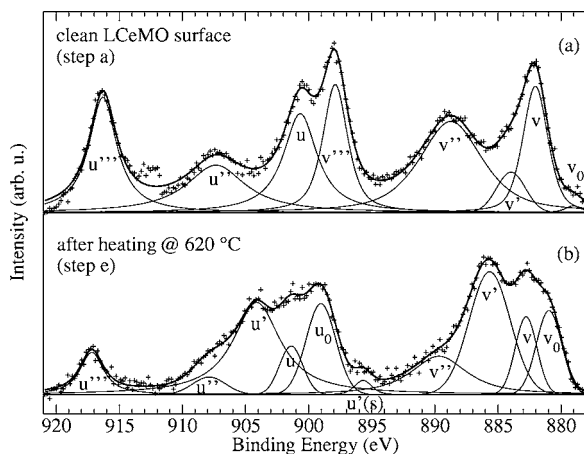
FIG. 4. (a) Ce $3d$ signals for the clean LCeMO surface (after step a in Table I) and (b) after heating at 620 °C (step e in Table I) after background subtraction. In accordance with the change of the Ce valence, the spectra have a clearly different shape. In curve (b) u'(s) denotes the $K\alpha_3$ satellite of u'.

pected, a typical Ce^{4+} spectrum; only the two strongest Ce^{3+} peaks can be discerned. The Ce^{3+} concentration is about 4%. A slight rise in the Ce^{3+} percentage to values around 10% occurs after steps $b-d$. The treatment steps e and f dramatically change the Ce valence towards the Ce^{3+} state, resulting in Ce^{3+} percentages of more than 50% for both cases. Figure 4(b) demonstrates the significantly different Ce $3d$ spectrum after treatment step e. It is interesting to note that also the O $1s$ peak shift is most dramatic after step e for LCeMO as well as for LCMO (see Fig. 3). The Ce valence change turns out to be reversible by reoxidation: The Ce^{3+} percentage shrinked to 6% after step g.

In LCMO, the Ca $2p$ signal is shifted by 0.3 eV towards higher binding energies after step c and by 1.0 eV after step e and moves back to the original position after step g.

In summary, an increased oxygen diffusion above approximately 600 °C may be assumed for both films.

D. The La $3d$ core level signal

The shape of the La $3d$ peaks is the same for LCMO and LCeMO and is similar to the shape found in the spectrum of La_2O_3.[59] The spin-orbit splitting is, as for La_2O_3, 16.8 eV for both samples and after all treatment steps (Fig. 5). However, the La $3d$ binding energy shifts in a steplike manner after step d for LCeMO (one step earlier than the dramatic change in the Ce valence) and after step e for LCMO (Fig. 6). In both cases the binding energy moves closer to the La_2O_3 value.[59] The steplike shift of the binding energy is larger for LCMO, as well as the corresponding O $1s$ shift is larger in that case. Furthermore, we note that for the clean surfaces the La $3d$ binding energies differ by 0.3 eV between LCMO and LCeMO; a similar difference is observed for the O $1s$ lines. Altogether, the behavior of the La $3d$ peak supports the assumption of an enhanced oxygen loss in both films after step e; for LCeMO the process might begin already with step d. For both samples, the La $3d$ peak moves back to the position
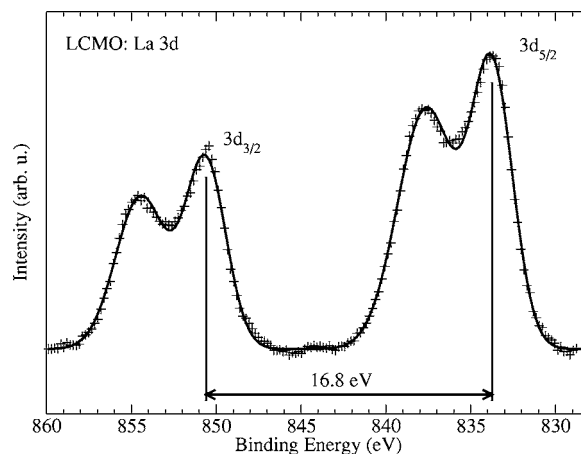
FIG. 5. La $3d$ signal of the cleaned LCMO surface after subtraction of the background and the $K\alpha_{3,4}$ satellites.

observed after steps a and b after the reoxidation procedure of step g.

We note that there is a common trend of the O $1s$, Ce $3d$, Ca $2p$, and La $3d$ lines: With progressive deoxygenation, they all move to higher binding energies. Apart from the fact that the shifts of the various core level lines may reflect changes in the individual binding conditions, their overall tendency towards higher binding energies is consistent with the Fermi level moving up in energy.[75] This is confirmed by the UPS measurements, which show that the work function decreases between treatment steps a and f by 1.7 eV for LCeMO and 1.0 eV for LCMO. Such a behavior is in fact expected in a simple semiconductor band model if a transition from p to n doping takes place. Hence, we may interpret these observations as a first hint that deoxygenation indeed changes the doping type. Much stronger evidence for this is provided by the analysis of the Mn valence described in the following sections.

E. The Mn $2p$ core level signal

To explore the Mn valence, the Mn core level signals should naturally provide the most relevant information. For a
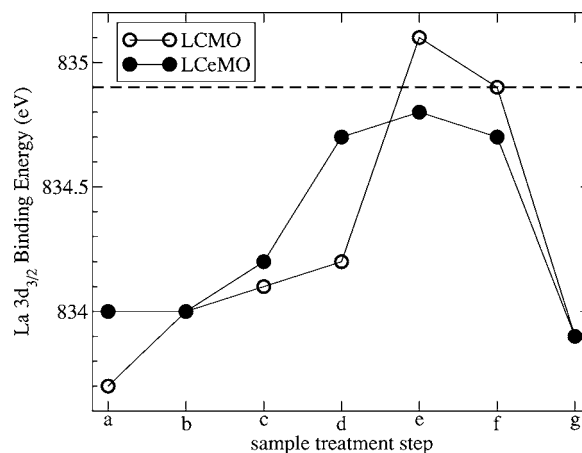
FIG. 6. Development of the La $3d_{3/2}$ binding energy after the different heating steps (Table I). The dashed line indicates the value for La_2O_3 (Ref. 59).
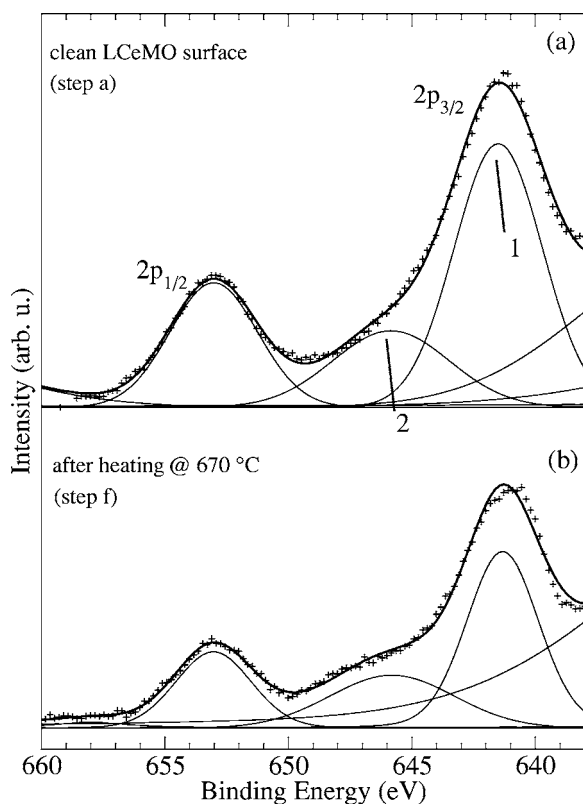
FIG. 7. Mn $2p$ doublet of the LCeMO film after the treatment steps a and f. The Mn $2p_{3/2}$ component is fit by two peaks (labeled 1 and 2), with peak 2 corresponding to the shake-up satellite in curve (b). The Mn $2p_{1/2}$ component is fit by only one peak as the corresponding shake-up satellite is too weak to be visible. The overlapping peaks on the low-binding-energy side originate from Auger lines, as discussed in the text.

good introduction into the complex problem of manganese XPS core level signals, see for example Ref. 41. First, we consider the Mn $2p$ doublet, inspired by an XPS investigation of Gao *et al.*[6] There, the Mn $2p$ doublet of $La_{0.9}Sn_{0.1}MnO_3$ exhibited a shift by 0.8 eV towards lower binding energies compared to the Mn $2p$ doublet of $La_{0.9}Ca_{0.1}MnO_3$, which was interpreted as evidence for a mixed $Mn^{2+/3+}$ state in $La_{0.9}Sn_{0.1}MnO_3$. However, another group[72] observed the same Mn $2p$ binding energy both for $LaMnO_3$ compounds doped with divalent as well as tetravalent ions and questioned the suitability of the Mn $2p$ signal for investigations of the Mn valence.

In our study, we see little or no energetic shift of the Mn $2p$ doublet, but we observe the formation of shake-up satellites, especially after step f, which are offset from the main peaks of the Mn $2p$ doublet by approximately 5 eV towards higher binding energies. In agreement with all peak changes described in Secs. III B–III D, the reoxidation drives the Mn $2p$ signal back to the shape which was observed after step a.

Figure 7 exemplarily shows the effect for the LCeMO film. For LCMO we find the satellite formation to be the same. This behavior is typical for Mn^{2+} systems such as MnO.[40,73,74] Thus, it is clear that deoxygenation by heating in UHV drives the LCeMO *and* the LCMO film from the original $Mn^{3+/4+}$ state towards a mixed $Mn^{2+/3+}$ state. The analysis
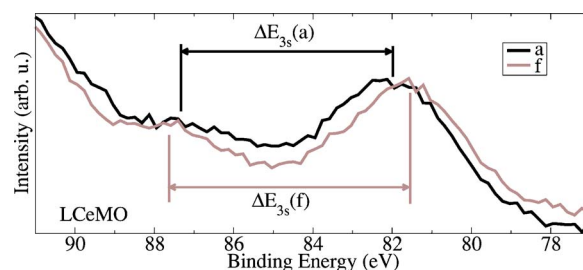
FIG. 8. (Color online) Mn $3s$ signals of the LCeMO film for the as-cleaned state (step a) and the heavily deoxygenated state (step f). The increase of the splitting energy is qualitatively visible, a quantitative analysis inevitably needs a fitting procedure due to the weakness of the signal and the neighboring strong La $4d$ satellite, as shown in Fig. 2.

of the Mn $3s$ signal will show this in a more pronounced and quantitative manner.

In summary, the development of the Mn $2p$ doublet provides clear evidence for the presence of Mn^{2+} ions and thus the formation of an electron-doped state in both films. In the case of LCeMO we have to keep in mind that the Ce valence changes simultaneously towards the Ce^{3+} state (see Fig. 4). This might indicate a phase separation process (which, however, is reversible as can be seen after step g). This assumption is supported by the strongly changed stoichiometry (see Table II) after step f for LCeMO. According to the chemical formula given there, the formal Mn valence is higher after step f than after step e, but the Mn $2p$ signal after step f suggests a Mn valence closer to 2+ than after step e. On the other hand, the changed stoichiometry is only of limited significance, since the stoichiometry determination, in the LCeMO case, is based on three uncertain atomic sensitivity factors, namely those of La, Ce and Mn. As the Mn and Ce valences change during the deoxygenation procedure, it is likely that also the atomic sensitivity factors change, which then produces a strongly but artificially changed stoichiometry. This is indeed observed after step f (Table II).

As a general result, we conclude that the Mn $2p$ signal can be used to get first qualitative information on the Mn valence of manganites: A lowering of the Mn valence is unambiguously visible by the formation of shake-up satellites at 5 eV from the main peaks.

F. Mn $3s$ exchange splitting

The value of the Mn $3s$ exchange splitting was used to determine the Mn valence in a more quantitative way than is possible by means of the Mn $2p$ signal. As described in the literature,[39,40] there is a linear relation between the Mn valence and the Mn $3s$ exchange splitting energy [Eq. (2)]. Figure 8 depicts the raw data of the Mn $3s$ doublet for LCeMO after the treatment steps a and f. One can clearly see that the exchange splitting has increased after step f. Because of the overlapping La $4d$ satellite and the rather low signal-to-noise ratio,[76] a quantitative evaluation is only possible by a fitting procedure as discussed in conjunction with Fig. 2. From the ΔE_{3s} values thus found, we calculated the Mn valences by means of Eq. (2) for both films after the different
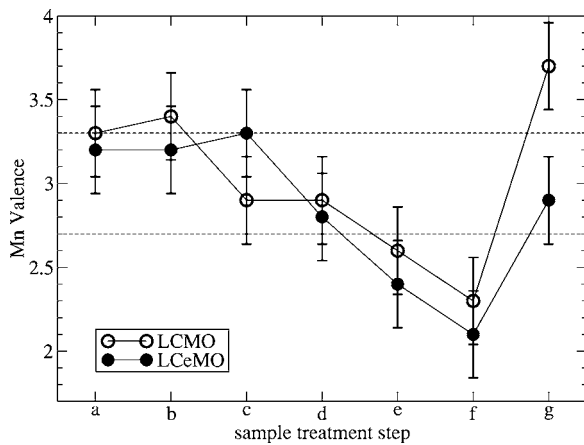
FIG. 9. Mn valences of the LCMO and LCeMO film as derived from Eq. (2) after the different heat treatment steps of Table I. The horizontal dashed lines indicate the nominal Mn valences: 3.3 for LCMO and 2.7 for LCeMO. Thus one can conclude that the LCMO film has a Mn valence very close to its nominal value already in the as-cleaned state, while the LCeMO film is overoxygenated in the as-cleaned state and reaches its nominal Mn valence only after deoxygenation, especially after step d.

FIG. 10. Plot of the Mn $3s$ exchange splitting energy versus the formal Mn valence, which was calculated by employing the stoichiometries from Table II, the corresponding Ce valences as determined from the Ce $3d$ signal, and fixed valences for the remaining elements (La^{3+}, Ca^{2+}, O^{2-}). Solid line: Linear fit to the experimental data of Galakhov et $al.$ (Ref. 39) for different mixed-valent manganite bulk samples; dashed line: Linear fit to the experimental data of Zhao et $al.$ (Ref. 40) for manganese oxides; vertical dotted lines: Formal Mn valences for stoichiometric $La_{0.7}Ca_{0.3}MnO_3$ and $La_{0.7}Ce_{0.3}MnO_3$, respectively. The data points are indexed according to the sample treatment steps of Table I. From point a to f the oxygen content is successively reduced; point g represents the reoxidized state.

treatment steps. The result is shown in Fig. 9. The data give clear evidence that, without heat treatment in UHV, i.e., after step a, the LCeMO film is *not* in the mixed $Mn^{2+/3+}$ state expected from the chemical formula of the compound. Instead, the Mn valence is similar in LCeMO and LCMO, close to the value expected for the nominal composition of the LCMO film. Figure 9 clearly shows that the oxygen out-diffusion induced by heating in UHV (steps $b-f$) lowers the Mn valence significantly in both cases down to values approaching +2. Finally, the reoxidation step g drives both films back to a state fairly close to the initial one. From the latter fact, it can be assumed that heating in an oxygen atmosphere, which constitutes the first part of *each* treatment step (see Table I), always essentially restores the state as reached after step a.

The error of the Mn valence is mainly caused by the error of the Mn $3s$ splitting value, which is assumed to be 0.2 eV for all data points. This value was derived from the peak fitting procedure, in which slight variations of the fit parameter constrains and of the background resulted in this uncertainty. The error bars thus mainly characterize the possible influence of systematic errors caused by the interfering La $4d$ satellite. Note that the change of ΔE_{3s} with heating temperature is expected to be less affected by such a systematic error than the absolute values.

As a check of consistency, another approach is chosen in Fig. 10. There, the Mn valences are derived from the stoichiometries of Table II under the assumption of charge neutrality. Despite the uncertainty of the stoichiometries, the formal Mn valences derived from them exhibit a clear correlation with the Mn $3s$ energy splitting. The data points of the present work are depicted along with the data available in the literature [the same data that provided Eq. (2)]. Within the error bars we find a good agreement. While Galakhov et $al.$[39] studied a wide variety of bulk manganese compounds having different formal Mn valences, we find the same linear rela-

tionship for one and the same manganite thin film when tuning its oxygen content.

For LCMO, the data demonstrates a clear increase of the Mn $3s$ exchange splitting with the decrease in Mn valence caused by the progressive rise in temperature. The correlation with the progression in heating temperature is not so clear for points c and d, which may be attributed to the large error of the formal Mn valence.

For LCeMO the same general tendency can be seen if we consider the points a and e. There are again fluctuations for the points between a and e. While in Fig. 9 point f for LCeMO fits well to the overall tendency set up by the other data points, this point shows a conspicuous deviation with regard to the formal Mn valence (Fig. 10). This can again be explained by the artificially changed stoichiometry, as discussed in detail in the previous section. As expected from the behavior of all other XPS signals, the reoxidation of the films (point g) is accompanied by a decrease in the Mn $3s$ splitting and an increase of the formal Mn valence. The original state (a) is recovered within the error bars.

In Fig. 10 the error of the Mn $3s$ splitting energy is assumed to be 0.2 eV, as explained above. Here, the more pronounced error is that of the formal Mn valence, as this uncertainty results from the error of the peak areas. This error is even roughly doubled if one additionally takes the following errors of the atomic sensitivity factors into consideration: $s_{La}=s_{Ce}=10\pm1$, $s_{Mn}=2.6\pm0.1$; the remaining atomic sensitivity factors were assumed to have negligible errors.

In summary, the evaluation of the Mn $3s$ splitting gives clear evidence that it is possible to prepare a mixed $Mn^{2+/3+}$ state and, consequently, electron doping in the outermost few

nanometers of divalent- and tetravalent-ion-doped lanthanum manganite thin films by decreasing their oxygen content.

IV. CONCLUSIONS

The Mn valence states of LCMO and LCeMO epitaxial thin films were studied by XPS for as-cleaned surfaces as well as for different deoxygenation states. The shape of the Mn 2p doublet and the value of the Mn 3s exchange splitting turned out to be valuable indicators of the Mn valence. Both compounds were found to be in a mixed Mn$^{3+/4+}$ state after a surface cleaning procedure in an O_2 atmosphere and before any deoxygenation treatment. Heating in ultrahigh vacuum resulted in oxygen loss which in both cases was accompanied by the transition towards a lower Mn valence between +2 and +3. For LCeMO not only the Mn valence changed, but also the Ce valence was driven from the 4+ state towards the 3+ state. The changes in the Mn and Ce valences could be reversed by heating in an oxygen atmosphere, which resulted in the reoxidation of the films. Finally, our investigation shows that even a standard XPS experiment using non-monochromatized x-rays is capable of determining the Mn valence state of manganite films very clearly. Therefore, the method provides an inexpensive characterization tool which can give valuable support in the process of optimizing the preparation of such films.

In general, heating in ultrahigh vacuum turned out to be a suitable method for tuning the Mn valence of lanthanum manganite thin films between a mixed 3+/4+ state and mixed 2+/3+ state and thus for preparing electron-doped manganite films. XPS allows monitoring the two coupled processes: The change of the oxygen content and the Mn valence change.

Concerning future investigations, it has to be tested whether the electron-doped state in LCeMO, which was prepared by heating in an ultrahigh vacuum, remains stable in air.

*Electronic address: elke@iapp.de

[1] J. M. D. Coey, M. Viret, and S. von Molnár, Adv. Phys. **48**, 167 (1999).

[2] A.-M. Haghiri-Gosnet and J.-P. Renard, J. Phys. D **36**, R127 (2003).

[3] M. B. Salamon and M. Jaime, Rev. Mod. Phys. **73**, 583 (2001).

[4] A. P. Ramirez, J. Phys.: Condens. Matter **9**, 8171 (1997).

[5] Z. W. Li, A. H. Morrish, and J. Z. Jiang, Phys. Rev. B **60**, 10284 (1999).

[6] J. Gao, S. Y. Dai, and T. K. Li, Phys. Rev. B **67**, 153403 (2003).

[7] X. Guo, S. Dai, Y. Zhou, Z. Chen, G. Yang, F. Liu, K. Ibrahim, and H. Qian, Mater. Sci. Eng., B **76**, 18 (2000).

[8] G. T. Tan, S. Y. Dai, P. Duan, Y. L. Zhou, H. B. Lu, and Z. H. Chen, J. Appl. Phys. **93**, 5480 (2003).

[9] G. T. Tan, P. Duan, S. Y. Dai, Y. L. Zhou, H. B. Lu, and Z. H. Chen, J. Appl. Phys. **93**, 9920 (2003).

[10] T. Yanagida, T. Kanki, B. Vilquin, H. Tanaka, and T. Kawai, J. Appl. Phys. **97**, 033905 (2005).

[11] J. Yang, B. C. Zhao, R. L. Zhang, Y. Q. Ma, Z. G. Sheng, W. H. Song, and Y. P. Sun, Solid State Commun. **132**, 83 (2004).

[12] S. Roy and N. Ali, J. Appl. Phys. **89**, 7425 (2001).

[13] V. L. Joseph Joly, P. A. Joy, and S. K. Date, J. Magn. Magn. Mater. **247**, 316 (2002).

[14] B. I. Min, S. K. Kwon, B. W. Lee, and J.-S. Kang, J. Electron Spectrosc. Relat. Phenom. **114-116**, 801 (2001).

[15] P. Mandal and S. Das, Phys. Rev. B **56**, 15073 (1997).

[16] J. R. Gebhardt, S. Roy, and N. Ali, J. Appl. Phys. **85**, 5390 (1999).

[17] B. W. Lee, K. Y. Seo, Y. J. Kim, H. Han, H. H. Lee, J. C. Han, S. Y. Park, and C. S. Kim, J. Magn. Magn. Mater. **226-230**, 803 (2001).

[18] W. J. Chang, C. C. Hsieh, J. Y. Juang, K. H. Wu, T. M. Uen, Y. S. Gou, C. H. Hsu, and J.-Y. Lin, J. Appl. Phys. **96**, 4357 (2004).

[19] T. Yanagida, T. Kanki, B. Vilquin, H. Tanaka, and T. Kawai, Solid State Commun. **129**, 785 (2004).

[20] A. Caneiro, L. Morales, F. Prado, R. D. Sachez, and A. Serquis, Phys. Rev. B **62**, 6825 (2000).

[21] R. Ganguly, I. K. Gopalakrishnan, and J. V. Yakhmi, J. Phys.: Condens. Matter **12**, L719 (2000).

[22] J. Philip and T. R. N. Kutty, J. Phys.: Condens. Matter **11**, 8537 (1999).

[23] J. E. Gayone, M. Abbate, G. Alejandro, D. G. Lamas, M. Tovar, and G. Zampieri, J. Alloys Compd. **369**, 252 (2004).

[24] M. P. de Jong, I. Bergenti, V. A. Dediu, M. Fahlman, M. Marsi, and C. Taliani, Phys. Rev. B **71**, 014434 (2005).

[25] M. F. Hundley and J. J. Neumeier, Phys. Rev. B **55**, 11511 (1997).

[26] P. Raychaudhuri, S. Mukherjee, A. K. Nigam, J. John, U. D. Vaisnav, R. Pinto, and P. Mandal, J. Appl. Phys. **86**, 5718 (1999).

[27] C. Mitra, P. Raychaudhuri, S. K. Dhar, A. K. Nigam, and R. Pinto, J. Magn. Magn. Mater. **226-230**, 809 (2001).

[28] C. Mitra, P. Raychaudhuri, J. John, S. K. Dhar, A. K. Nigam, and R. Pinto, J. Appl. Phys. **89**, 524 (2001).

[29] C. Mitra, P. Raychaudhuri, G. Köbernik, K. Dörr, K.-H. Müller, L. Schultz, and R. Pinto, Appl. Phys. Lett. **79**, 2408 (2001).

[30] H. Chou, Z. Y. Hong, S. J. Sun, J. Y. Juang, and W. J. Chang, J. Appl. Phys. **97**, 10A308 (2005).

[31] C. Mitra, P. Raychaudhuri, K. Dörr, K.-H. Müller, L. Schultz, P. M. Oppeneer, and S. Wirth, Phys. Rev. Lett. **90**, 017202 (2003).

[32] P. Raychaudhuri, C. Mitra, P. D. A. Mann, and S. Wirth, J. Appl. Phys. **93**, 8328 (2003).

[33] T. Yanagida, T. Kanki, B. Vilquin, H. Tanaka, and T. Kawai, Phys. Rev. B **70**, 184437 (2004).

[34] S. W. Han, J.-S. Kang, K. H. Kim, J. D. Lee, J. H. Kim, S. C. Wi, C. Mitra, P. Raychaudhuri, S. Wirth, K. J. Kim, B. S. Kim, J. I. Jeong, S. K. Kwon, and B. I. Min, Phys. Rev. B **69**, 104406 (2004).

[35] C. Mitra, Z. Hu, P. Raychaudhuri, S. Wirth, S. I. Csiszar, H. H. Hsieh, H.-J. Lin, C. T. Chen, and L. H. Tjeng, Phys. Rev. B **67**, 092404 (2003).

[36] S. W. Han, J. D. Lee, K. H. Kim, C. Mitra, J. I. Jeong, K. J. Kim, B. S. Kim, B. I. Min, J. H. Kim, S. C. Wi, and J.-S. Kang, Phys. Status Solidi B **241**, 1577 (2004).

[37] K. Asokan, J. C. Jan, K. V. R. Rao, J. W. Chiou, H. M. Tsai, S. Mookerjee, W. F. Pong, M.-H. Tsai, R. Kumar, S. Husain, and J. P. Srivastava, J. Phys.: Condens. Matter **16**, 3791 (2004).

[38] J.-W. Lin, W. J. Chang, J. Y. Juang, T. M. Wen, K. H. Wu, Y. S. Gou, J. M. Lee, and J. M. Chen, J. Magn. Magn. Mater. **282**, 237 (2004).

[39] V. R. Galakhov, M. Demeter, S. Bartkowski, M. Neumann, N. A. Ovechkina, E. Z. Kurmaev, N. I. Lobachevskaya, Y. M. Mukowskii, J. Mitchell, and D. L. Ederer, Phys. Rev. B **65**, 113102 (2002).

[40] L. Z. Zhao and V. Young, J. Electron Spectrosc. Relat. Phenom. **34**, 45 (1984).

[41] A. J. Nelson, J. G. Reynolds, and J. W. Roos, J. Vac. Sci. Technol. A **18**, 1072 (2000).

[42] A. Kowalczyk, A. Ślebarski, A. Szajek, J. Baszyński, and A. Winiarski, J. Magn. Magn. Mater. **212**, 107 (2000).

[43] M. P. de Jong, V. A. Dediu, C. Taliani, and W. R. Salaneck, J. Appl. Phys. **94**, 7292 (2003).

[44] B. Holzapfel, B. Roas, L. Schultz, P. Bauer, and G. Saemann-Ischenko, Appl. Phys. Lett. **62**, 3178 (1992).

[45] J. Choi, H. Dulli, S.-H. Liou, P. A. Dowben, and M. A. Langell, Phys. Status Solidi B **214**, 45 (1999).

[46] J. Choi, J. Zhang, S.-H. Liou, P. A. Dowben, and E. W. Plummer, Phys. Rev. B **59**, 13453 (1999).

[47] H. Dulli, P. A. Dowben, S.-H. Liou, and E. W. Plummer, Phys. Rev. B **62**, R14629 (2000).

[48] J.-J. Liang and H.-S. Weng, Ind. Eng. Chem. Res. **32**, 2563 (1993).

[49] Y. Zhang-Steenwinkel, J. Beckers, and A. Bliek, Appl. Catal., A **235**, 79 (2002).

[50] S. Ponce, M. A. Peña, and J. L. G. Fierro, Appl. Catal., B **24**, 193 (2000).

[51] P. Decorse, G. Caboche, and L.-C. Dufour, Solid State Ionics **117**, 161 (1999).

[52] K. Dörr, J. M. de Teresa, K.-H. Müller, D. Eckert, T. Walter, E. Vlakhov, K. Nenkov, and L. Schultz, J. Phys.: Condens. Matter **12**, 7099 (2000).

[53] D. A. Shirley, Phys. Rev. B **5**, 4709 (1972).

[54] R. Kwok, XPSPEAK 4.1 (2000), http://www.phy.cuhk.edu.hk/~surface/XPSPEAK/.

[55] *Practical Surface Analysis by Auger and X-ray Photoelectron Spectroscopy*, edited by D. Briggs and M. P. Seah (Wiley, New York, 1983).

[56] W.-Y. Howng and R. J. Thorn, Chem. Phys. Lett. **56**, 463 (1978).

[57] *CRC Handbook of Chemistry and Physics*, 81st ed., edited by D. R. Lide (CRC Press, Boca Raton, 2001).

[58] S. Tougaard, J. Vac. Sci. Technol. A **14**, 1415 (1996).

[59] *Handbook of X-ray photoelectron spectroscopy*, edited by G. E. Muilenberg (Perkin-Elmer Corporation, Eden Prairie, Minnesota, 1979).

[60] W. Zhang, X. Wang, and I. W. Boyd, Appl. Phys. Lett. **73**, 2745 (1998).

[61] *Surface Analysis by Auger and X-ray Photoelectron Spectroscopy*, edited by D. Briggs and J. T. Grant (IM Publications and SurfaceSpectra Limited, Chichester, 2003).

[62] P. Decorse, E. Quenneville, S. Poulin, M. Meunier, A. Yelon, and F. Morin, J. Vac. Sci. Technol. A **19**, 910 (2001).

[63] O. Gunnarsson and K. Schönhammer, Phys. Rev. B **28**, 4315 (1983).

[64] J. C. Fuggle, F. U. Hillebrecht, Z. Zołnierek, R. Lässer, C. Freiburg, O. Gunnarsson, and K. Schönhammer, Phys. Rev. B **27**, 7330 (1983).

[65] E. Wuilloud, B. Delley, W.-D. Schneider, and Y. Baer, Phys. Rev. Lett. **53**, 202 (1984).

[66] W.-D. Schneider, B. Delley, E. Wuilloud, J.-M. Imer, and Y. Baer, Phys. Rev. B **32**, 6819 (1985).

[67] M. Coldea, M. Neumann, S. Lütkehoff, S. Mähl, and R. Coldea, J. Alloys Compd. **278**, 72 (1998).

[68] D. R. Mullins, S. H. Overbury, and D. R. Huntley, Surf. Sci. **409**, 307 (1998).

[69] E. J. Peisler, O. J. Marsh, R. A. Beach, and T. C. McGill, J. Vac. Sci. Technol. B **19**, 1611 (2001).

[70] T. Toliński, A. Kowalczyk, M. Pugaczowa-Michalska, and G. Chełkowska, J. Phys.: Condens. Matter **15**, 1397 (2003).

[71] F. Zhang, P. Wang, J. Koberstein, S. Khalid, and S.-W. Chan, Surf. Sci. **563**, 74 (2004).

[72] J.-S. Kang, Y. J. Kim, C. G. Olson, and B. I. Min, J. Phys.: Condens. Matter **13**, 3779 (2001).

[73] M. Oku, K. Hirokawa, and S. Ikeda, J. Electron Spectrosc. Relat. Phenom. **7**, 465 (1975).

[74] H.-K. Hu and J. W. Rabalais, Surf. Sci. **107**, 376 (1981).

[75] Note that binding energies provided by an XPS measurement are always referred to the Fermi level.

[76] The stronger peak of the Mn 3s doublet is roughly 40 times lower in height than the O 1s peak, and is superimposed on a background that is 3.7 times higher than the peak itself.